ISSN 1560-3547, Regular and Chaotic Dynamics, 0000, Vol. 00, No. 0, pp. 1–21. © RCD Editorial Office, 2016.

Finite time collapse of three point vortices in the plane

Vikas S. Krishnamurthy[1*] and Mark A. Stremler[2]**

[1] *Erwin Schrodinger International Institute for Mathematics and Physics*
Boltzmangasse 9, 1090 Vienna, Austria

[2] *Department of Biomedical Engineering and Mechanics*
460 Turner Street NE, Suite 304, Blacksburg, VA 24061, U. S. A.

Received July 8, 2018; accepted Month XX, 20XX

Abstract—We investigate the finite-time collapse of three point vortices in the plane utilizing the geometric formulation of three vortex motion from Krishnamurthy, Aref & Stremler (2018) Phys. Rev. Fluids **3**, 024702. In this approach, the vortex system is described in terms of the interior angles of the triangle joining the vortices, the circle that circumscribes that triangle, and the orientation of the triangle. Symmetries in the governing geometric equations of motion for the general three-vortex problem allow us to consider a reduced parameter space in the relative vortex strengths. The well-known conditions for three-vortex collapse are reproduced in this formulation, and we show that these conditions are necessary and sufficient for the vortex motion to consist of collapsing or expanding self-similar motion. The geometric formulation enables a new perspective on the details of this motion. Relationships are determined between the interior angles of the triangle, the vortex strength ratios, the (finite) system energy, the time of collapse, and the distance traveled by the configuration prior to collapse. Several illustrative examples of both collapsing and expanding motion are given.

MSC2010 numbers: 70F07, 70K99, 76B47

DOI: 10.0000/S1560354700000012

Keywords: ideal flow, vortex dynamics, point vortices

1. INTRODUCTION

The Euler equation describing the motion of an inviscid and incompressible fluid has several exact solutions in the classical theory of fluid dynamics [7, 18]. One important exact solution is the finite dimensional system of N point vortices in planar two-dimensional flow [21, 28] that was introduced by Helmholtz 160 years ago [13]. The motion of three point vortices holds a special place within the theory of vortex dynamics owing to the fact that it is an integrable system with a variety of non-trivial relative motions [2]. The dynamics of three point vortices has been explored independently by several authors, starting with Gröbli's 19th century thesis [12], and with several others replicating and adding to the analysis during the second half of the 20th century [1, 3, 22, 27, 31]; an accounting of the early history of the three-vortex problem can be found in [6].

Self-similar motion of three vortices is an especially interesting case in which, for a particular set of initial vortex positions and strengths, the triangle formed by the vortices moves without changing shape and the vortices converge to a single point in a finite time. The phenomenon of finite time collapse has been known since the earliest solutions to the three vortex problem [12, 31]. Various aspects of finite time collapse have been studied using the classical formulations summarized in §2.1, including the conditions required for collapse [5, 14] and stability properties of the collapse solutions [5, 32]. The dynamics of three point vortices near collapse has also been investigated, with 'near collapse' defined as a slight perturbation of the initial conditions and vortex strengths necessary for collapse [19].

*E-mail: vikas.krishnamurthy2@gmail.com
**E-mail: stremler@vt.edu

In addition to its intrinsic interest as a point vortex problem, the importance of finite-time collapse solutions in two-dimensions arises from the appearance of related motion for three smooth vortices. Given a sufficiently smooth initial velocity field, there exists for all time a smooth velocity field as the solution of the incompressible Euler equation [30], and collapse is not possible. Obviously, the finite-time collapse solution for point vortices does not contradict this result since the point vortex velocity field is not smooth, but singular, at any instant of time. However, it is interesting to note that a smooth initial velocity distribution corresponding to three vortices of finite size (which do not overlap each other) may be constructed such that these vortices follow the trajectories of three point vortices undergoing collapse for a significant duration of the motion [33]. Assume the vortex centroids of the finite sized vortices are initially at the positions corresponding to three collapsing point vortices. They follow the collapsing point vortex trajectories quite closely until the distances between the vortex centroids is of the same order as the vortex size, at which point their trajectories diverge from the collapsing trajectories [33].

In this paper, we utilize a geometrical reformulation of the three vortex problem [16] to systematically study finite-time collapse. In §2.1 we provide the background theory of three vortex dynamics found in the classical literature, and in §2.2 we recall the ODEs in the recently developed geometrical formulation [16] of three vortex motion. In §2.3, we study some of the symmetries in these geometrical ODEs that reduce the parameter space of the three vortex problem. In §3.1, we show that finite time collapse of three vortices is necessarily self-similar and derive the necessary and sufficient conditions for self-similar motion. In §3.2 we show that the symmetries in the system allow us to focus on a reduced region of parameter space in our study of self-similar motion of three point vortices. In §3.3 we discuss the dependence of the vortex strengths and configuration Hamiltonian energy on the triangle geometry. In §3.4 we discuss the collapse/expansion time of the configuration as a function of the geometry and show that this time can also be determined as a function of the Hamiltonian energy of the system. In §3.5, we reconstruct the motions of the three vortices as a function of time using the geometric formulation and determine the distance traveled by the circumcenter during self-similar motion as a representation of the magnitude of the vortex motion. We discuss a few selected examples of vortex collapse and expansion in §3.6 and conclude in §4.

2. THE DYNAMICS OF THREE POINT VORTICES

2.1. Classical equations of motion

The motion of the three point vortices in an otherwise quiescent potential flow on the plane is governed by a system of six nonlinear ordinary differential equations (ODEs). These six equations determine the evolution of the positions of the three vortices given in Cartesian co-ordinates by (x_α, y_α), $\alpha = 1, 2, 3$. Let the flow plane be regarded as the complex z-plane and the positions of the vortices be denoted by $z_\alpha = x_\alpha + \mathrm{i}y_\alpha$ for $\alpha = 1, 2, 3$. If we denote the strengths of the three vortices by $\Gamma_\alpha \neq 0$, $\alpha = 1, 2, 3$, then the symmetric functions of the vortex strengths

$$\gamma_1 = \Gamma_1 + \Gamma_2 + \Gamma_3, \tag{2.1a}$$

$$\gamma_2 = \Gamma_1\Gamma_2 + \Gamma_2\Gamma_3 + \Gamma_3\Gamma_1, \tag{2.1b}$$

$$\gamma_3 = \Gamma_1\Gamma_2\Gamma_3, \tag{2.1c}$$

play an important role in classifying three vortex motion and formulating the governing equations. The three ODEs for the motion of the three point vortices are [7, 18, 21, 28]

$$\overline{\frac{\mathrm{d}z_1}{\mathrm{d}t}} = \frac{1}{2\pi\mathrm{i}}\left(\frac{\Gamma_2}{z_1 - z_2} + \frac{\Gamma_3}{z_1 - z_3}\right), \tag{2.2a}$$

$$\overline{\frac{\mathrm{d}z_2}{\mathrm{d}t}} = \frac{1}{2\pi\mathrm{i}}\left(\frac{\Gamma_1}{z_2 - z_1} + \frac{\Gamma_3}{z_2 - z_3}\right), \tag{2.2b}$$

$$\overline{\frac{\mathrm{d}z_3}{\mathrm{d}t}} = \frac{1}{2\pi\mathrm{i}}\left(\frac{\Gamma_1}{z_3 - z_1} + \frac{\Gamma_2}{z_3 - z_2}\right), \tag{2.2c}$$

where the bar denotes complex conjugation. It is clear from (2.2) that the case of self-similar collapse leads to singular vortex velocities in a finite time.

Within the six-dimensional system of ODEs (2.2), a three dimensional system of equations for the three inter-vortex distances s_α, defined by

$$s_1 = |z_2 - z_3|, \quad s_2 = |z_3 - z_1|, \quad s_3 = |z_1 - z_2|, \tag{2.3}$$

can be isolated [12, 31]. These three ODEs are

$$\frac{\mathrm{d}s_1^2}{\mathrm{d}t} = \frac{2\Delta}{\pi}\Gamma_1\frac{s_3^2 - s_2^2}{s_2^2 s_3^2}, \qquad \frac{\mathrm{d}s_2^2}{\mathrm{d}t} = \frac{2\Delta}{\pi}\Gamma_2\frac{s_1^2 - s_3^2}{s_3^2 s_1^2}, \qquad \frac{\mathrm{d}s_3^2}{\mathrm{d}t} = \frac{2\Delta}{\pi}\Gamma_3\frac{s_2^2 - s_1^2}{s_1^2 s_2^2}, \tag{2.4a}$$

where the area of the vortex triangle, Δ, is given by Heron's formula [9]

$$16\Delta^2 = 2s_2^2 s_3^2 + 2s_3^2 s_1^2 + 2s_1^2 s_2^2 - s_1^4 - s_2^4 - s_3^4. \tag{2.4b}$$

The sign of Δ on the right-hand-side of the ODEs in (2.4a) is defined to be positive or negative according to whether the three vortices 123 are oriented anti-clockwise or clockwise, respectively. At instants of time when the vortex configuration becomes colinear, the description (2.4) is incomplete, and a separate ODE for Δ has to be consulted to 'continue' the evolution past such instants. This ODE for Δ is [8]

$$\frac{\mathrm{d}\Delta}{\mathrm{d}t} = \frac{1}{8\pi}\left[(\Gamma_1+\Gamma_2)\frac{s_1^2 - s_2^2}{s_3^2} + (\Gamma_2+\Gamma_3)\frac{s_2^2 - s_3^2}{s_1^2} + (\Gamma_3+\Gamma_1)\frac{s_3^2 - s_1^2}{s_2^2}\right]. \tag{2.5}$$

A qualitative picture of three vortex motion for different initial conditions and vortex strengths may be obtained by considering (2.4) and (2.5) together with the sign of γ_2 (2.1). We refer the interested reader to the cited literature for the derivation and discussion of these results [8, 12, 31].

The system of equations (2.2) is a Hamiltonian system [7, 18, 21, 28], with the Hamiltonian given by

$$H = -\frac{1}{4\pi}(\Gamma_1\Gamma_2 \log|z_1 - z_2|^2 + \Gamma_2\Gamma_3 \log|z_2 - z_3|^2 + \Gamma_3\Gamma_1 \log|z_3 - z_1|^2); \tag{2.6}$$

it may be verified that the equations of motion (2.2) can be written as

$$\Gamma_\alpha\overline{\frac{\mathrm{d}z_\alpha}{\mathrm{d}t}} = 2\mathrm{i}\frac{\partial H}{\partial z_\alpha}, \quad \alpha = 1, 2, 3. \tag{2.7}$$

The Hamiltonian is interpreted as the finite part of the kinetic energy of the fluid [7, 18]. As with the vortex velocities in (2.2), the Hamiltonian (2.6) becomes singular at the time of collapse. However, we see that if all the vortex positions overlap at some instant of time, then the three logarithmic singularities that are formed in (2.6) may be 'removed' from H—if they are all equal—by imposing the condition $\gamma_2 = 0$, with γ_2 defined as in (2.1). This condition is discussed in detail in §3.1.

The Hamiltonian system has several independent constants of motion apart from the Hamiltonian (2.6) itself. These other constants of motion are the two components of linear impulse, Q and P, written conveniently in complex form as

$$Q + \mathrm{i}P = \Gamma_1 z_1 + \Gamma_2 z_2 + \Gamma_3 z_3, \tag{2.8}$$

and the angular impulse I

$$I = \Gamma_1|z_1|^2 + \Gamma_2|z_2|^2 + \Gamma_3|z_3|^2. \tag{2.9}$$

It may be verified directly from (2.2) that $Q + \mathrm{i}P$ and I are constants of motion. A different but not independent integral of motion, L, may be obtained by combining I, Q and P as

$$L = \gamma_1 I - Q^2 - P^2 = \Gamma_1\Gamma_2|z_1 - z_2|^2 + \Gamma_2\Gamma_3|z_2 - z_3|^2 + \Gamma_3\Gamma_1|z_3 - z_1|^2. \tag{2.10}$$

The center of vorticity for the three vortices is defined in terms of the linear impulse, for $\gamma_1 \neq 0$, as

$$z_{cv} = \frac{Q + \mathrm{i}P}{\gamma_1}. \tag{2.11}$$

One can, if desired, shift the vortex positions so that $z_{cv} = 0$.

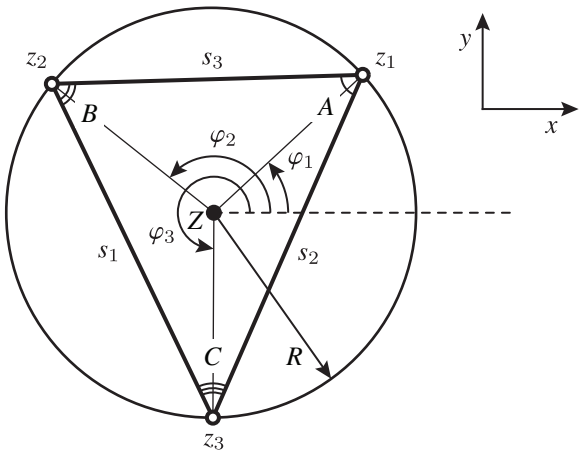

Fig. 1. A geometrical picture of three vortex motion, where the geometrical variables in the dynamically evolving vortex triangle are tracked. This is equivalent to the dynamical evolution of the vortex positions, except for those instants when the vortex configuration becomes colinear. The details of this formulation are based on the assumption that the vortices are arranged in an anti-clockwise orientation, as shown here. This figure has been reproduced with permission from [16].

2.2. Geometrical equations of motion

A geometrical picture of three vortex motion emerges from the simple observation that for any three points in the plane forming a triangle, a circumcircle can always be defined which passes through these three points [4]. The 'geometrical variables' are then the radius of the circumcircle, the position of the center of the circumcircle (i.e., the circumcenter), the interior angles of the vortex triangle, and the orientation of the vortex triangle in the plane. In this formulation, these geometric variables are tracked in time instead of tracking the vortex positions z_α via (2.2). This geometrical description of three vortex dynamics was developed in detail in [16], and in this section we summarize the equations of motion for this approach.

Consider the change of variables

$$z_1 = Z + R\mathrm{e}^{\mathrm{i}\varphi_1}, \qquad z_2 = Z + R\mathrm{e}^{\mathrm{i}\varphi_2}, \qquad z_3 = Z + R\mathrm{e}^{\mathrm{i}\varphi_3}, \tag{2.12}$$

where R is the circumradius and Z is the position of the circumcenter, as shown in Fig. 1. The angles φ_1, φ_2 and φ_3 are the angles made by the vortices at z_1, z_2 and z_3, respectively, relative to a horizontal axis passing through Z. Without any loss of generality we assume that the three vortices are arranged in an anti-clockwise fashion as shown in Fig. 1, so that the interior angles of the vortex triangle A, B, C are related to φ_α by

$$\varphi_2 - \varphi_1 = 2C, \qquad \varphi_3 - \varphi_2 = 2A, \qquad \varphi_1 - \varphi_3 = 2B - 2\pi. \tag{2.13a}$$

The interior angles A, B and C have to satisfy the geometrical constraint

$$A + B + C = \pi. \tag{2.13b}$$

If A, B and C are known, then (2.13) can be inverted to give φ_1, φ_2 and φ_3 if one of the three angles φ_α is also known; throughout this paper we choose to use φ_1 to represent the orientation of the vortex triangle. Knowing Z, R, A, B, C and φ_1, we can then reconstruct the vortex positions z_α from (2.12) and (2.13).

We can derive ODEs for R, Z, A, B, C and φ_1 by using (2.2) together with (2.12) and (2.13). The details of this derivation are found in [16], and here we present only the final equations:

$$\frac{\mathrm{d}R^2}{\mathrm{d}t} = \frac{1}{4\pi}\Big[\Gamma_1 \cot B \cot C(\cot B - \cot C) + \Gamma_2 \cot C \cot A(\cot C - \cot A) + \Gamma_3 \cot A \cot B(\cot A - \cot B)\Big], \tag{2.14a}$$

$$\cot A\frac{\mathrm{d}A}{\mathrm{d}t} = \frac{1}{8\pi R^2}\Big[\Gamma_1(1-\cot B\cot C)(\cot B-\cot C) - \Gamma_2\cot C\cot A(\cot C-\cot A) - \Gamma_3\cot A\cot B(\cot A-\cot B)\Big], \quad (2.14b)$$

$$\cot B\frac{\mathrm{d}B}{\mathrm{d}t} = \frac{1}{8\pi R^2}\Big[\Gamma_2(1-\cot C\cot A)(\cot C-\cot A) - \Gamma_3\cot A\cot B(\cot A-\cot B) - \Gamma_1\cot B\cot C(\cot B-\cot C)\Big], \quad (2.14c)$$

$$\cot C\frac{\mathrm{d}C}{\mathrm{d}t} = \frac{1}{8\pi R^2}\Big[\Gamma_3(1-\cot A\cot B)(\cot A-\cot B) - \Gamma_1\cot B\cot C(\cot B-\cot C) - \Gamma_2\cot C\cot A(\cot C-\cot A)\Big], \quad (2.14d)$$

$$\frac{\mathrm{d}Z}{\mathrm{d}t} = \frac{R\mathrm{e}^{\mathrm{i}\varphi_1}}{4\pi\Delta}\Big[\Gamma_1\left(\mathrm{e}^{-\mathrm{i}B}\cot C\sin B-\mathrm{e}^{\mathrm{i}C}\cot B\sin C\right) + \Gamma_2\left(\mathrm{e}^{\mathrm{i}C}\cot A\sin C-\mathrm{e}^{\mathrm{i}A}\cot C\sin A+2\mathrm{i}\,\mathrm{e}^{-\mathrm{i}B}\sin A\cos C\right) + \Gamma_3\left(\mathrm{e}^{-\mathrm{i}A}\cot B\sin A-\mathrm{e}^{-\mathrm{i}B}\cot A\sin B+2\mathrm{i}\,\mathrm{e}^{\mathrm{i}C}\sin A\cos B\right)\Big], \quad (2.14e)$$

$$\frac{\mathrm{d}\varphi_1}{\mathrm{d}t} = \frac{1}{4\pi\Delta}\Big[\Gamma_1\big(\cot B\,\sin^2 C+\cot C\,\sin^2 B\big) + \Gamma_2\big(\cot C\,\sin^2 A-\cot A\,\sin^2 C+\sin 2A\big) + \Gamma_3\big(\cot B\,\sin^2 A-\cot A\,\sin^2 B+\sin 2A\big)\Big]. \quad (2.14f)$$

The area of the vortex triangle appearing in (2.14e) and (2.14f) is given by [16]

$$|\Delta| = 2R^2\,\sin A\,\sin B\,\sin C. \quad (2.15)$$

At instants of time when the vortices are colinear, we have $\Delta = 0$, $A, B, C = 0$ or π, and $R \to \infty$. Thus, as with the formulation in (2.4), the system (2.14) cannot be used to continue the evolution of a vortex triangle through a colinear state. In contrast to the formulation in (2.4), however, it is not possible to have a continuation of the solution via addition of an equation for $\mathrm{d}\Delta/\mathrm{d}t$ owing to the singularities that occur at these instants; one must instead return to (2.2) to continue the triangle evolution through the colinearity.

The constants of motion H and L defined in (2.6) and (2.10) can be written in terms of R, A, B and C by using the relations

$$s_1 = 2R\sin A, \qquad s_2 = 2R\sin B, \qquad s_3 = 2R\sin C \quad (2.16)$$

to get

$$L = 4\gamma_3 R^2\left(\frac{\sin^2 A}{\Gamma_1}+\frac{\sin^2 B}{\Gamma_2}+\frac{\sin^2 C}{\Gamma_3}\right), \quad (2.17a)$$

$$H = -\frac{1}{2\pi}\left[\gamma_2\log\frac{R}{R_0}+\gamma_3\left(\frac{\log\sin A}{\Gamma_1}+\frac{\log\sin B}{\Gamma_2}+\frac{\log\sin C}{\Gamma_3}\right)\right], \quad (2.17b)$$

where R_0 is a constant length scale, and we have used the freedom of choosing a constant in the Hamiltonian without altering the equations of motion.

The full system of equations (2.14) along with the constraint (2.13b) provides a six-dimensional system of ODEs, as expected for the three vortex system. Within this system of equations we have a four-dimensional subsystem consisting of (2.14a), (2.14b), (2.14c) and (2.14d), along with the three constraints (2.13b), (2.17a) and (2.17b). This reduced system of ODEs for R, A, B and C is therefore an integrable system of equations within the full three vortex system.

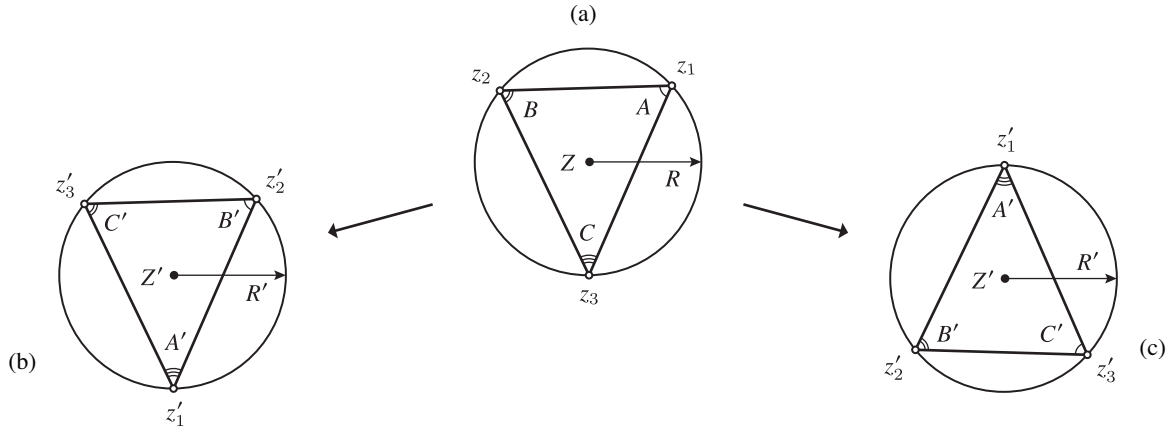

Fig. 2. Transformation of (a) the original vortex triangle under (b) clockwise rotation of the vortex labels given by (2.18) and (c) reflection of the configuration about the x axis given by (2.20).

2.3. Symmetries in the governing equations

As a result of symmetries in the governing equations (2.14), not every choice of the vortex strengths and triangle geometry leads to unique system behavior. Symmetries may take the form of a simple permutation of the vortex indices, which does not change the physical system. They can also take the form of a change in the triangle orientation or a change in the sign of all circulations, both of which correspond to physical changes. These symmetries, described in detail below, can be applied in any combination.

Consider first a permutation of the vortex labels that leaves the physical characteristics of the system unchanged. Since the formulation in §2.2 does not allow for a clockwise orientation of the labels, all permutations must be a rotation of the labels. Assume the labels are rotated clockwise, giving the 'new' configuration shown in Figure 2(b) with

$$\begin{aligned} \Gamma_1' = \Gamma_3, \quad z_1' = z_3, \quad A' = C, \quad \varphi_1' = \varphi_3, \\ \Gamma_2' = \Gamma_1, \quad z_2' = z_1, \quad B' = A, \quad \varphi_2' = \varphi_1, \\ \Gamma_3' = \Gamma_2, \quad z_3' = z_2, \quad C' = B, \quad \varphi_3' = \varphi_2, \end{aligned} \tag{2.18a}$$

where the primes indicate the parameters and variables in the relabeled system. The location and size of the circumcircle have not changed, so that $Z' = Z$ and $R' = R$. Applying this transformation (2.18a) to the equations of motion (2.14), together with (2.13), gives

$$\begin{gathered} \frac{\mathrm{d}(R')^2}{\mathrm{d}t} = \frac{\mathrm{d}R^2}{\mathrm{d}t}, \quad \frac{\mathrm{d}A'}{\mathrm{d}t} = \frac{\mathrm{d}C}{\mathrm{d}t}, \quad \frac{\mathrm{d}B'}{\mathrm{d}t} = \frac{\mathrm{d}A}{\mathrm{d}t}, \quad \frac{\mathrm{d}C'}{\mathrm{d}t} = \frac{\mathrm{d}B}{\mathrm{d}t}, \\ \frac{\mathrm{d}\varphi_1'}{\mathrm{d}t} = \frac{\mathrm{d}\varphi_3}{\mathrm{d}t} = \frac{\mathrm{d}\varphi_1}{\mathrm{d}t} - 2\frac{\mathrm{d}B}{\mathrm{d}t}, \quad \frac{\mathrm{d}Z'}{\mathrm{d}t} = \frac{\mathrm{d}Z}{\mathrm{d}t}, \end{gathered} \tag{2.18b}$$

demonstrating that the motions of these two configurations are equivalent. This transformation does not change the symmetric functions of the vortex strengths (2.1) and the key system constants L and H (2.17), giving

$$\gamma_1' = \gamma_1, \quad \gamma_2' = \gamma_2, \quad \gamma_3' = \gamma_3, \quad L' = L, \quad H' = H. \tag{2.18c}$$

An anti-clockwise rotation of the labels is equivalent to two clockwise rotations. Thus, the dynamics of any vortex triangle is invariant to a rotation of the vortex labels, as one should expect. Note that the final equality in (2.18b) is difficult to show from (2.14e) and is seen more easily by applying the transformation to a form of (2.14e) that mixes the geometric and complex variables (see equation (27b) in [16]), namely

$$\frac{\mathrm{d}Z}{\mathrm{d}t} = \frac{1}{8\pi \mathrm{i}\Delta}\left[(Q + \mathrm{i}P)\left(\cot A + \cot B + \cot C\right) - \gamma_1\left(z_1 \cot A + z_2 \cot B + z_3 \cot C\right)\right]. \tag{2.19}$$

Consider now the case in which the vortex configuration is reflected about the x axis, as illustrated in Figure 2(c). In order to maintain an anti-clockwise orientation for the transformed vortex locations so that we can apply the formulation in §2.2, two of the reflected vortices must be relabeled. In anticipation of applying this transformation to self-similar motion in §3.2, we represent this reflection as

$$\begin{aligned} \Gamma_1' &= -\Gamma_3, \quad z_1' = \overline{z_3}, \quad A' = C, \quad \varphi_1' = 2\pi - \varphi_3, \\ \Gamma_2' &= -\Gamma_2, \quad z_2' = \overline{z_2}, \quad B' = B, \quad \varphi_2' = 2\pi - \varphi_2, \\ \Gamma_3' &= -\Gamma_1, \quad z_3' = \overline{z_1}, \quad C' = A, \quad \varphi_3' = 2\pi - \varphi_1. \end{aligned} \tag{2.20a}$$

One can think of this transformation as viewing the configuration 'from behind'. The size of the circumcircle remains unchanged, so $R' = R$, but the circumcenter becomes $Z' = \overline{Z}$. Applying this transformation (2.20a) to the equations of motion (2.14) and (2.19), together with (2.13a), gives

$$\begin{gathered} \frac{\mathrm{d}(R')^2}{\mathrm{d}t} = \frac{\mathrm{d}R^2}{\mathrm{d}t}, \quad \frac{\mathrm{d}A'}{\mathrm{d}t} = \frac{\mathrm{d}C}{\mathrm{d}t}, \quad \frac{\mathrm{d}B'}{\mathrm{d}t} = \frac{\mathrm{d}B}{\mathrm{d}t}, \quad \frac{\mathrm{d}C'}{\mathrm{d}t} = \frac{\mathrm{d}A}{\mathrm{d}t}, \\ \frac{\mathrm{d}\varphi_1'}{\mathrm{d}t} = -\frac{\mathrm{d}\varphi_3}{\mathrm{d}t} = -\left(\frac{\mathrm{d}\varphi_1}{\mathrm{d}t} - 2\frac{\mathrm{d}B}{\mathrm{d}t}\right), \quad \frac{\mathrm{d}Z'}{\mathrm{d}t} = \frac{\mathrm{d}\overline{Z}}{\mathrm{d}t}, \end{gathered} \tag{2.20b}$$

and the motions are reflectionally symmetric, as expected. In this case, the symmetric functions of vortex strengths and the key constants become

$$\gamma_1' = -\gamma_1, \quad \gamma_2' = \gamma_2, \quad \gamma_3' = -\gamma_3, \quad L' = L, \quad H' = H. \tag{2.20c}$$

Thus we see that a full representation of the three-vortex dynamics can be determined by exploring only a subset of the full $(\gamma_1, \gamma_2, \gamma_3)$ parameter space; for example, one can, without any loss of generality, restrict attention to those configurations for which $\gamma_3 > 0$, with all other configurations given by a reflection of these cases.

Finally, consider changing the signs on all of the vortices without changing their locations, giving

$$\begin{aligned} \Gamma_1' &= -\Gamma_1, \quad z_1' = z_1, \quad A' = A, \quad \varphi_1' = \varphi_1, \\ \Gamma_2' &= -\Gamma_2, \quad z_2' = z_2, \quad B' = B, \quad \varphi_2' = \varphi_2, \\ \Gamma_3' &= -\Gamma_3, \quad z_3' = z_3, \quad C' = C, \quad \varphi_3' = \varphi_3. \end{aligned} \tag{2.21a}$$

Applying this transformation (2.21a) to the equations of motion (2.14) and (2.19), and using (2.13a), gives

$$\begin{gathered} \frac{\mathrm{d}(R')^2}{\mathrm{d}t} = -\frac{\mathrm{d}R^2}{\mathrm{d}t}, \quad \frac{\mathrm{d}A'}{\mathrm{d}t} = -\frac{\mathrm{d}A}{\mathrm{d}t}, \quad \frac{\mathrm{d}B'}{\mathrm{d}t} = -\frac{\mathrm{d}B}{\mathrm{d}t}, \quad \frac{\mathrm{d}C'}{\mathrm{d}t} = -\frac{\mathrm{d}C}{\mathrm{d}t}, \\ \frac{\mathrm{d}\varphi_1'}{\mathrm{d}t} = -\frac{\mathrm{d}\varphi_1}{\mathrm{d}t}, \quad \frac{\mathrm{d}Z'}{\mathrm{d}t} = -\frac{\mathrm{d}Z}{\mathrm{d}t}, \end{gathered} \tag{2.21b}$$

and the symmetric functions of vortex strengths and the system constants again become

$$\gamma_1' = -\gamma_1, \quad \gamma_2' = \gamma_2, \quad \gamma_3' = -\gamma_3, \quad L' = L, \quad H' = H. \tag{2.21c}$$

Therefore, changing the signs on all three of the vortices is equivalent to reversing time in the equations of motion.

3. SELF-SIMILAR MOTION OF THREE POINT VORTICES

3.1. Necessary and sufficient conditions for self-similar motion and finite time collapse

It has been known since the very first investigation of three vortex motion [6, 12] that taking $L = 0$ and $\gamma_2 = 0$ leads to self-similar motion. Here we show that $L = 0$, $\gamma_2 = 0$ are both necessary and sufficient for the self-similar motion of three point vortices in an approach that complements the analysis of Aref [5].

Consider the case in which the three point vortices collapse into a single point at some finite time $t = \tau > 0$, so that $z_1(\tau) = z_2(\tau) = z_3(\tau)$. In terms of the geometric variables, the condition

at collapse may be expressed as $R(\tau) = 0$. Then, since L given by (2.17a) is a constant of motion, we must have $L = 0$ as a necessary condition for collapse. Since $R(t) \neq 0$ for $t \neq \tau$, this condition becomes

$$\frac{\sin^2 A(t)}{\Gamma_1} + \frac{\sin^2 B(t)}{\Gamma_2} + \frac{\sin^2 C(t)}{\Gamma_3} = 0, \tag{3.1}$$

where it has been emphasized that the angles $A(t)$, $B(t)$ and $C(t)$ may vary with time. This equation shows that in order to have real-valued solutions for $A(t)$, $B(t)$ and $C(t)$, the vortex strengths cannot all be of the same sign. From the expression (2.17b) for the Hamiltonian of the three vortex system we find, by taking exponentials on both sides, that

$$\exp(-2\pi H/\gamma_3) = (R(t)/R_0)^{\gamma_2/\gamma_3} \left(\sin A(t)\right)^{1/\Gamma_1} \left(\sin B(t)\right)^{1/\Gamma_2} \left(\sin C(t)\right)^{1/\Gamma_3}. \tag{3.2}$$

We note that we must always have $\exp(-2\pi H/\gamma_3) > 0$. For the condition $R(\tau) = 0$ to be consistent with (3.2), we must have either that $\gamma_2 = 0$, or

$$\left(\sin A(t)\right)^{1/\Gamma_1} \left(\sin B(t)\right)^{1/\Gamma_2} \left(\sin C(t)\right)^{1/\Gamma_3} \sim \left(1/R(t)\right)^{\gamma_2/\gamma_3} \quad \text{as} \quad t \to \tau. \tag{3.3}$$

Since not all vortex strengths are of the same sign, (3.3) could be true if one of the angles goes to zero or π. In a three vortex collision, this corresponds to the remaining two angles also going to zero or π and the vortices becoming colinear. A colinear vortex configuration corresponds to $R \to \infty$, contradicting $R(\tau) = 0$. Therefore (3.3) can never be true, and we conclude that $\gamma_2 = 0$ is a necessary condition for three-vortex collapse.

Let us consider the possibility that only two of the vortices—say vortex 1 and vortex 2—collide at some instant of time $\tau > 0$, with vortex 3 remaining separate. This situation corresponds to $C(t)$ tending to zero as $t \to \tau$, while $A(t)$, $B(t)$, and $R(t)$ remain finite (as $t \to \tau$). This contradicts (3.2), and we conclude that a two vortex collision in a three vortex system is not a possible solution.

We have so far established that $L = 0$ and $\gamma_2 = 0$ are necessary conditions for three-vortex collapse in a finite time $\tau > 0$; we now show that these conditions are also sufficient. Assuming $L = 0$ leads to equation (3.1). We get from (2.17b) and assuming $\gamma_2 = 0$ that

$$H = -\frac{\gamma_3}{2\pi}\left(\frac{\log\sin A(t)}{\Gamma_1} + \frac{\log\sin B(t)}{\Gamma_2} + \frac{\log\sin C(t)}{\Gamma_3}\right). \tag{3.4}$$

In a three-dimensional $(\sin A, \sin B, \sin C)$ space, (2.13b), (3.1) and (3.4) define three surfaces that intersect at most at isolated points. Therefore when assuming $L = 0$ and $\gamma_2 = 0$ we can only have solutions where the angles A, B and C are constant in time. If A, B and C are constants, then from (2.14a), we have

$$\frac{\mathrm{d}R^2}{\mathrm{d}t} = k_1, \tag{3.5}$$

where k_1 is a constant. Note that if we take $A = B = C$, then by (2.14a) we have $k_1 = 0$ and thus $R =$ constant, which is the special case of relative equilibria of three point vortices discussed in [16]. Under the assumption that $R(\tau) = 0$, the solution to (3.5) is

$$R(t) = R_0\sqrt{1 - \frac{t}{\tau}}, \tag{3.6}$$

where we have chosen the length scale $R_0 = R(0)$ and the constant $k_1 = -R_0^2/\tau < 0$. We have thus shown that the necessary and sufficient conditions for finite time collapse are $L = 0$ and $\gamma_2 = 0$, with $\tau > 0$.

If the angles in the vortex triangle are constants and the circumradius is time dependent, then the motion has to be self-similar. We thus conclude that the only possible form of finite time collapse is self-similar collapse. Given a set of vortex strengths Γ_1, Γ_2 and Γ_3 compatible with $\gamma_2 = 0$, a vortex configuration (defined by A, B and C) that collapses can always be found as the points of intersection of (2.13b), (3.1) and (3.4).

We have so far considered only $\tau > 0$, which means that the vortex configuration collapses to a point at $t = \tau$. We can also consider $\tau < 0$, corresponding to $k_1 > 0$. We see from (3.5) that if

$k_1 > 0$ then R always increases with time, with $R(\tau) = 0$. Since A, B and C are constants, $\tau < 0$ corresponds to self-similar expansion and τ is interpreted as the time-scale of expansion. Thus, in general we have that $L = 0$ and $\gamma_2 = 0$ are necessary and sufficient conditions for self-similar motion of the vortex triangle, with the sign of τ determining whether that motion is collapsing or expanding.

3.2. Symmetries in self-similar motion

Self-similar motion of a vortex triangle can be parameterized by a single scalar. Since $\gamma_2 = 0$, there must be at least one vortex with positive circulation (and at least one with negative circulation). Without any loss of generality, we can assign the vortex labels such that $\Gamma_1 > 0$ and work in terms of the vortex strength ratio

$$g = \Gamma_1/\Gamma_2; \tag{3.7a}$$

by (2.1) (with $\gamma_2 = 0$) we also have

$$\Gamma_1/\Gamma_3 = -(g+1), \quad \Gamma_2/\Gamma_3 = -(g+1)/g. \tag{3.7b}$$

We assume that the strengths of all three vortices are non-zero and finite, giving three values of g that correspond to singularities: taking $g \to \pm\infty$ corresponds to having $\Gamma_1 \to \infty$ and/or $\Gamma_2, \Gamma_3 \to 0$; if $g = 0$, then $\Gamma_1 = \Gamma_3 = 0$ and/or $\Gamma_2 \to \pm\infty$; and if $g = -1$, then $\Gamma_1 = \Gamma_2 = 0$ and/or $\Gamma_3 \to \pm\infty$. All other values of g are allowed.

The observations in §2.3 enable us to limit the range of g that must be considered for determining unique self-similar motion. Consider first the case of two positive vortices and one negative vortex. By choice we assign the labels so that $\Gamma_1 > 0$ and vortices 2 and 3 are arranged in an anti-clockwise orientation. If $\Gamma_3 > 0$, then by (3.7) we have $g < -1$, and we rotate the system labels clockwise using the transformation (2.18), so that in the relabeled system we have $\Gamma_1' = \Gamma_3 > 0$ and $\Gamma_3' = \Gamma_2 < 0$ with the strength ratio

$$g' = \Gamma_1'/\Gamma_2' = \Gamma_3/\Gamma_1 = -1/(g+1) > 0. \tag{3.8}$$

Since the vortex motion is invariant to this rotation of labels, every self-similar motion with $g < -1$ corresponds under rotation of labels to a self-similar motion with $g > 0$, and we can, without any loss of generality, restrict our attention to $g > -1$.

Consider now the case of two positive vortices with $g > 0$, corresponding to $\Gamma_1, \Gamma_2 > 0$ and $\Gamma_3 < 0$. If we reflect the configuration about the x axis, the reflected configuration has two negative vortices; we again choose for the (only) positive vortex to be labeled as vortex 1, and label the remaining vortices in an anti-clockwise direction. This transformation, given by (2.20), gives the new strength ratio

$$g' = \Gamma_1'/\Gamma_2' = \Gamma_3/\Gamma_2 = -g/(g+1); \tag{3.9}$$

since $g > 0$ we have $-1 < g' < 0$. Thus, without any loss of generality, we can restrict our attention to configurations consisting of $\Gamma_1 > 0$ and $\Gamma_2, \Gamma_3 < 0$, for which $-1 < g < 0$; all other configurations are related to one of these cases under a physical reflection and/or a rotation of labels. Note that $-1 < g < 0$ with $\Gamma_1 > 0$ gives $\gamma_3 > 0$.

Finally, consider changing the signs on all of the vortices without changing their locations, as given by the transformation (2.21). Assume we start with a configuration that has $\Gamma_1 > 0$ and $-1 < g < 0$. After a sign change, the new configuration has $\Gamma_1' < 0$, $\Gamma_2' > 0$, $\Gamma_3' > 0$ and $g' = g$, with motion equivalent to that of the initial system under the reversal of time. Applying two clockwise rotations (2.18) gives a transformed configuration with $\Gamma_1'' = \Gamma_2' > 0$, $\Gamma_2'' = \Gamma_3' > 0$, and $\Gamma_3'' = \Gamma_1' < 0$, for which

$$g'' = -(g+1)/g > 0. \tag{3.10}$$

We know this double-prime configuration has motion symmetric to that in a reflected system with $-1 < g''' < 0$ under the (additional) reflective transformation in (2.20). This combination of transformations gives

$$\begin{gathered} \Gamma_1''' = \Gamma_1, \quad \Gamma_2''' = \Gamma_3, \quad \Gamma_3''' = \Gamma_2, \\ A''' = A, \quad B''' = C, \quad C''' = B \end{gathered} \tag{3.11a}$$

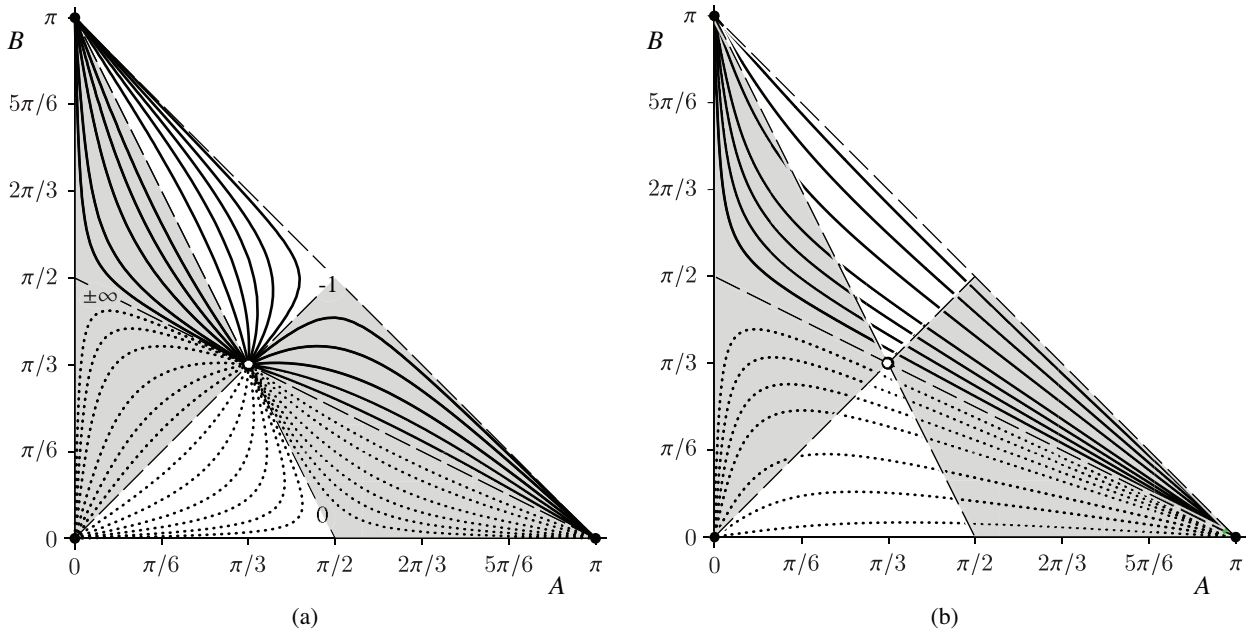

Fig. 3. Level curves of (a) g and (b) $\tilde{H}$ in the (A, B) plane, with $C = \pi - A - B$, that lead to self-similar motion. Solid lines show collapsing solutions and dotted lines show expanding solutions; dashed lines are the singular cases described in the text and are labeled according to the value of g in panel (a). Open circles mark the parameters for the equilateral triangle equilibrium configuration; solid circles are the colinear cases. The unshaded regions correspond to $-1 < g < 0$.

and the vortex strength ratio

$$g''' = -g''/(g''+1) = -(g+1). \tag{3.11b}$$

Thus, for every configuration with $-1 < g < 0$, changing the sign of every vortex and then rotating and reflecting the configuration leads to symmetric vortex motion with time reversed. That is, every collapsing (expanding) configuration with $\Gamma_1 > 0$ and strength ratio $-1 < g < 0$ is equivalent under reflection, rotation, and reversal of time to an expanding (collapsing) configuration with $\Gamma_1 > 0$ and $-1 < g''' < 0$, and these two configurations have the same value of the Hamiltonian, $H''' = H$.

3.3. Angle dependence on strength ratio and energy

Equations (3.1) and (3.4) for L and H, respectively, allow us to determine (numerically) the angle values that correspond to a collapsing or expanding configuration. Equation (3.1) can be interpreted as defining level curves of g (when $L = 0$). Applying (2.1) and using the condition $A + B + C = \pi$ to eliminate C in (3.1) gives

$$g = -\frac{\sin(B)\,\sin(2A+B)}{\sin(A)\,\sin(A+2B)} = -\frac{1-\cot^2 A - 2\cot A \cot B}{1-\cot^2 B - 2\cot A \cot B}. \tag{3.12}$$

Equation (3.12) defines a one parameter family of curves in A-B space, parameterized by g and shown in Fig. 3(a), for which self-similar solutions exist. The lines $A = B$ $(\neq C)$ and $A + B = \pi$ (equivalently, $C = 0$) give $g = -1$, the lines $2A + B = \pi$ (equivalently, $A = C \neq B$) and $B = 0$ give $g = 0$, and the lines $A + 2B = \pi$ (equivalently, $B = C \neq A$) and $A = 0$ correspond to $g \to \pm\infty$. Since these conditions correspond to singularities in the vortex strengths (see §3.2), it follows, in particular, that self-similar motions do not exist for isosceles triangle configurations (see also §3.4). These singular lines meet at the point $A = B = C = \pi/3$, which corresponds to the rotating equilibria discussed in [16]. As discussed in §3.2, we can assume without any loss of generality that $-1 < g < 0$ with $\Gamma_1 > 0$. This restriction limits the accessible space in the (A, B) plane to the unshaded regions in Fig. 3. Note that the line $A + 2B = \pi$ delineates the collapsing and expanding solutions in (A, B)-space, as indicated in Fig. 3(a,b) and discussed in §3.4.

Next, applying (2.1) and using the condition $A+B+C=\pi$ to eliminate C in (3.4) gives

$$\log\left[\frac{\sin A}{\sin(A+B)}\right]+g\log\left[\frac{\sin B}{\sin(A+B)}\right]=-g\,(g+1)\,\tilde{H} \tag{3.13a}$$

or

$$\log\left[\frac{1+\cot^2 B}{(\cot A+\cot B)^2}\right]+g\log\left[\frac{1+\cot^2 A}{(\cot A+\cot B)^2}\right]=-2g(g+1)\tilde{H}, \tag{3.13b}$$

where $\tilde{H}=-2\pi H/\Gamma_1^2$ is a dimensionless form of the Hamiltonian. We can combine (3.13a) with (3.12) to find $\tilde{H}$ as a function of only A and B, giving

$$\tilde{H}=\frac{\sin(A)\,\sin(A+2B)}{\sin^2 B-\sin^2 A}\left\{\log\left[\frac{\sin B}{\sin(A+B)}\right]-\frac{\sin(A)\,\sin(A+2B)}{\sin(B)\,\sin(2A+B)}\log\left[\frac{\sin A}{\sin(A+B)}\right]\right\}. \tag{3.13c}$$

Level curves in the (A,B) plane corresponding to $\tilde{H}=$ constant in (3.13c) are shown in Fig. 3(b). The intersections of these level curves with the lines $A=B$ and $2A+B=\pi$ are isolated singularities.

Note that although the Hamiltonian H (2.17b) is invariant to the transformations considered in §2.3 and §3.2, the dimensionless Hamiltonian $\tilde{H}$ (3.13) is not invariant because Γ_1 is used in the non-dimensionalization. The values of $\tilde{H}$ reported in this manuscript assume $-1<g<0$ with $\Gamma_1>0$; applying these results to a system that does not satisfy these assumptions requires a corresponding transformation of $\tilde{H}$.

3.4. Collapsing/expanding time for self-similar motion

Expressions for τ in terms of A, B, C and the vortex strengths can be obtained from (2.14b), (2.14c) and (2.14d). These expressions are [16]

$$-\frac{4\pi R_0^2}{\tau}=\Gamma_1(\cot B-\cot C)=\Gamma_2(\cot C-\cot A)=\Gamma_3(\cot A-\cot B). \tag{3.14}$$

These relationships can not hold for any isosceles triangle configuration with finite vortex strengths, in which case they do not give a unique value for τ. Thus, the restriction on isosceles triangles noted in §3.3 can also be seen from the expressions (3.14), which are algebraically symmetric between A, B and C.

We can introduce the dimensionless time parameter

$$\tilde{\tau}=\frac{\tau\Gamma_1}{4\pi R_0^2}; \tag{3.15a}$$

with $\Gamma_1>0$, $\tilde{\tau}>0$ (<0) corresponds to self-similar collapse (expansion). In combination with (3.14) and (3.7) this definition gives

$$\tilde{\tau}=\frac{\Gamma_1/\Gamma_3}{\cot B-\cot A}=\frac{g+1}{\cot A-\cot B}. \tag{3.15b}$$

Combining (3.15) with (3.12) enables us to determine $\tilde{\tau}$ as a function of A,B independent of the vortex strengths, giving

$$\tilde{\tau}=-\frac{\sin B\;\sin(A+B)}{\sin(A+2B)}. \tag{3.15c}$$

Figure 4(a) shows level curves corresponding to constant values of $\tilde{\tau}$ in (3.15c); the self-similar motion of triangles with angles (A,B,C), with $C=\pi-A-B$, lying on a given curve all have the same time of collapse or expansion. The self-similar time scale τ (3.14), and hence $\tilde{\tau}$ (3.15), is singular when $A=B$, $A+2B=\pi$ (i.e. $B=C$), or $2A+B=\pi$ (i.e. $A=C$). It is seen from (3.15c) that $\tilde{\tau}$, and hence τ, is positive or negative according to whether $A+2B>\pi$ or $A+2B<\pi$. The line $A+2B=\pi$ therefore delineates the collapsing and expanding solutions in (A,B)-space, as

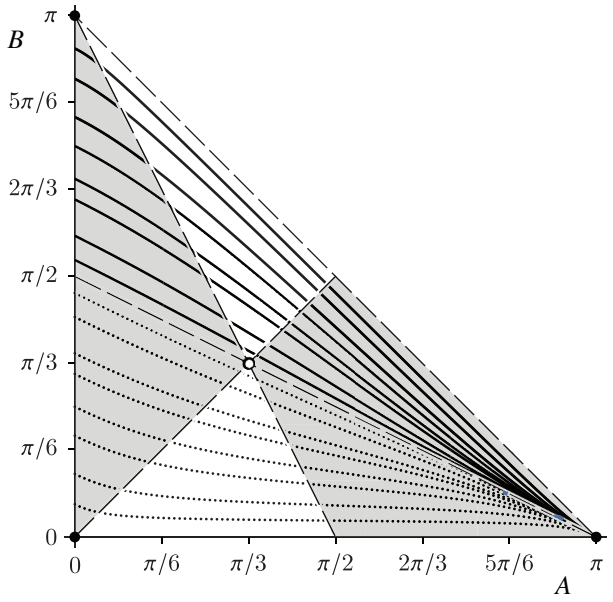

Fig. 4. Level curves of $\tilde{\tau}$ as a function of the angles A and B (with $C = \pi - A - B$) that lead to self-similar motion; solid lines show collapsing solutions and dotted lines show expanding solutions. Dashed lines are the singular cases described in the text. The open circle is the equilateral triangle equilibrium configuration; solid circles are the colinear cases. The unshaded portions of the graph correspond to $-1 < g < 0$.

indicated in Figs. 3 and 4. The intersections of the level curves in Fig. 4(a) with the lines $A = B$ and $2A + B = \pi$ are isolated singularities.

With this geometric approach it is also possible to determine the time $\tilde{\tau}$ as a function of $\tilde{H}$ and g. First, use (3.15) to eliminate $\cot B$ from (3.12) and obtain a quadratic equation for $\cot A$, which has the solution

$$3\tilde{\tau}\cot A = (2g+1) + (-1)^n\sqrt{g\,(g+1) + 1 + 3\tilde{\tau}^2}, \tag{3.16a}$$

where n is an integer. With $-1 < g < 0$ we have $0 < A < \pi/2$, for which $\cot A > 0$, and the inequalities

$$2g + 1 - \sqrt{g^2+g+1} < 0 < 2g + 1 + \sqrt{g^2+g+1}.$$

Thus, even values of n give $\tilde{\tau} > 0$ and odd values of n give $\tilde{\tau} < 0$. Similarly, eliminating $\cot A$ from (3.12) gives

$$3\tilde{\tau}\cot B = -(g+2) + (-1)^n\sqrt{g\,(g+1) + 1 + 3\tilde{\tau}^2}, \tag{3.16b}$$

with n again an integer. If we assume $-1 < g < 0$ and $\tilde{\tau} > 0$, then $\pi/3 < B < \pi$ and the left hand side of (3.16b) changes sign as B is varied, with a zero at $B = \pi/2$. The right hand side of (3.16b) changes sign as g is varied only when n is even; it is strictly negative when n is odd, as is $\tilde{\tau}\cot B$ when $\tilde{\tau} < 0$. Thus, we again see that even values of n give $\tilde{\tau} > 0$ and odd values of n give $\tilde{\tau} < 0$. We can therefore make the substitution $(-1)^n = \mathrm{sgn}(\tilde{\tau})$ in (3.16), where $\mathrm{sgn}(x)$ is the signum function. Equations (3.16) can be rewritten as

$$9\tilde{\tau}^2(1 + \cot^2 A) = [f_g(\tilde{\tau}) + g - 1]\,[f_g(\tilde{\tau}) + g + 2]\,, \tag{3.17a}$$

$$9\tilde{\tau}^2(1 + \cot^2 B) = [f_g(\tilde{\tau}) + g - 1]\,[f_g(\tilde{\tau}) - 2g - 1]\,, \tag{3.17b}$$

$$9\tilde{\tau}^2(\cot A + \cot B)^2 = [f_g(\tilde{\tau}) + g - 1]^2\,, \tag{3.17c}$$

where

$$f_g(\tilde{\tau}) = 2\,\mathrm{sgn}(\tilde{\tau})\sqrt{3\tilde{\tau}^2 + g^2 + g + 1}. \tag{3.18}$$

By substituting (3.17) into (3.13b) we arrive at an implicit equation for $\tilde{\tau}(\tilde{H};g)$ given by

$$F(\tilde{\tau};g) = G(\tilde{H};g), \tag{3.19a}$$

where

$$F(\tilde{\tau};g) = \frac{[f_g(\tilde{\tau})-2g-1]\,[f_g(\tilde{\tau})+g+2]^g}{[f_g(\tilde{\tau})+g-1]^{(g+1)}} \tag{3.19b}$$

and

$$G(\tilde{H};g) = \exp\left[-2g(g+1)\tilde{H}\right]. \tag{3.19c}$$

In general, there are two solutions of (3.19) (with (3.18)) corresponding to whether $\tilde{\tau}$ is positive or negative. According to the transformation (3.11), there is a symmetry between collapsing and expanding configurations: they are related by $g' = -(g+1)$ and $\tilde{H}' = \tilde{H}$. Applying this transformation to (3.18) and (3.19) and taking $\tilde{\tau}' = -\tilde{\tau}$, we find that

$$f_{g'}(\tilde{\tau}') = -f_g(\tilde{\tau}), \quad F(\tilde{\tau}';g') = F(\tilde{\tau};g), \quad G(\tilde{H}';g') = G(\tilde{H};g), \tag{3.20}$$

so that the solutions of equation (3.19) are unchanged. Therefore, the two solutions of (3.19) for $\pm\tilde{\tau}$ correspond to the collapsing and expanding configurations that are related by the symmetry in (3.11).

A few special cases of (3.19) are worth considering. If $g = -1/2$, (i.e. $\Gamma_2 = \Gamma_3 = -2\Gamma_1$), then (3.18) and (3.19) become

$$\frac{f^2_{-1/2}(\tilde{\tau})}{f^2_{-1/2}(\tilde{\tau}) - 9/4} = e^{\tilde{H}}, \quad f^2_{-1/2}(\tilde{\tau}) = 3(4\tilde{\tau}^2+1), \tag{3.21a}$$

which can be solved explicitly for $\tilde{\tau}$ to give

$$\tilde{\tau}(\tilde{H};-1/2) = \pm\frac{1}{4}\left[\frac{3}{e^{\tilde{H}}-1} - 1\right]^{1/2}. \tag{3.21b}$$

Both collapsing and expanding solutions are given by (3.21) since the transformation (3.11) leaves g invariant if $g = -1/2$. When $g \to 0$ we have

$$\lim_{g\to 0}\tilde{H} = \lim_{g\to 0}\left\{\frac{\log\left[F(\tilde{\tau};g)\right]}{-2g(g+1)}\right\} \to \frac{0}{0};$$

applying l'Hôpital's rule gives

$$\lim_{g\to 0}\tilde{H} = \frac{1}{2}\left\{\frac{3}{f_0(\tilde{\tau})-1} + \log\left[\frac{f_0(\tilde{\tau})-1}{f_0(\tilde{\tau})+2}\right]\right\}, \tag{3.22a}$$

with

$$f_0(\tilde{\tau}) = 2\,\mathrm{sgn}(\tilde{\tau})\sqrt{3\tilde{\tau}^2+1}. \tag{3.22b}$$

Equation (3.22) gives an implicit expression for $\tilde{\tau}(\tilde{H};g)$ in the limit $g \to 0$. It may be verified that taking the limit $g \to -1$ produces the same result as (3.22) after a change in the sign of $\tilde{\tau}$, as expected from the transformation (3.11).

A plot of $\tilde{\tau} > 0$ as a function of $\tilde{H}$ is shown in Fig. 5a,b for various values of g. Solution curves for $\tilde{\tau}(\tilde{H};g) < 0$ can be obtained by reflecting the results in Fig. 5a,b about the $\tilde{\tau} = 0$ axis and taking $\tilde{H} \mapsto \tilde{H}$, $g \mapsto -(g+1)$. In Fig. 5a it might appear that the limiting cases $g \to 0$ and $g \to -1$ form an 'outer envelope' for the curves with parameter values $-1 < g < 0$. However, this is not the case, as seen clearly in Fig. 5b.

Figure 5(a) shows $\tilde{\tau} \to 0$ as $\tilde{H} \to \tilde{H}_{\max}(g)$, where $\tilde{H}_{\max}(g)$ is the maximum value of $\tilde{H}$ for a given value of g. This limit corresponds to the configuration becoming colinear, in which case the unscaled collapse time, τ from (3.14), becomes infinite. The behavior of $\tilde{\tau}$ is tied to the choice of

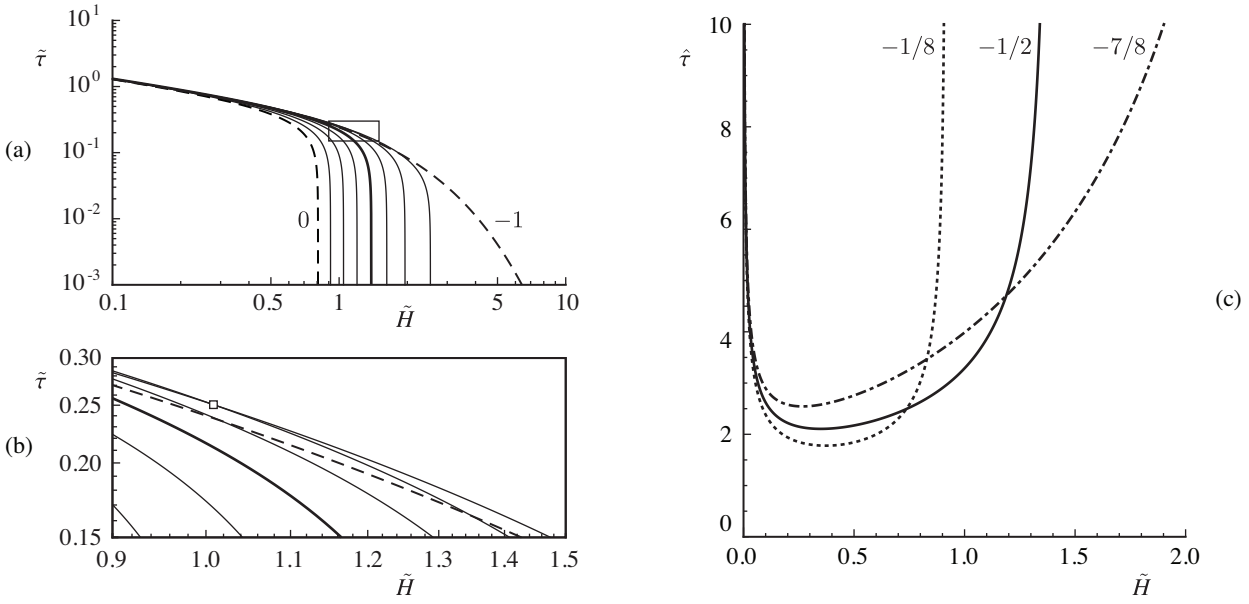

Fig. 5. (a,b) Dependence of $\tilde{\tau}$ on $\tilde{H}$; curves are shown for $g = -j/8$, $j = 0, ..., 8$. Dashed lines are the special cases $g = -1, 0$ and are labeled in (a) according to the value of g; the heavy solid line is the special case $g = -1/2$. Panel (b) shows the boxed region in (a). The square in (b) marks the point at which the curves for $g = -3/4$ and $g = -7/8$ intersect, giving $\tilde{H} \approx 1.009$ and $\tilde{\tau} \approx 0.250$. (c) Dependence of the rescaled $\hat{\tau}$ on $\tilde{H}$; example curves are labeled according to the corresponding value of g.

R_0 as the characteristic length in the scaling (3.15a); for a fixed value of R_0, it is seen from (2.16) that the separations between the vortices become zero as the configuration becomes colinear. In this situation one may wish to scale τ instead by one of the vortex separations; combining (2.16) and (3.15a) gives, for example,

$$\hat{\tau} = \frac{\tau \Gamma_1}{\pi s_{3,0}^2} = \frac{\tilde{\tau}}{\sin^2 C}, \tag{3.23}$$

where $s_{3,0}$ is the distance between vortices 1 and 2 at time $t = 0$. Since $\hat{\tau}$ mixes the two geometric representations, it does not appear possible to obtain an implicit mathematical relationship between $\hat{\tau}$ and $\tilde{H}$, but $\hat{\tau}(\tilde{H})$ can be determined numerically, as shown in Fig. 5(c). When the vortex separations are kept finite, the collapse time $\hat{\tau}$ becomes infinite as the vortex configuration approaches both the equilateral and colinear configurations. The $g = -1/2$ curve in Fig. 5(c) can be compared qualitatively with Kudela [17] who found, using a series of numerical experiments, a representation for $\tau(H)$ when $(\Gamma_1, \Gamma_2, \Gamma_3) = (-2, -2, 1)$.

For given values of $\tilde{\tau}$ (or $\hat{\tau}$) and $\tilde{H}$, equation (3.19) can be a multivalued function of g, as seen by the intersecting curves in Fig. 5b,c. That is, given any two strength ratios g and $\hat{g}$, there exist two corresponding vortex configurations undergoing self-similar motion that have the same characteristic time of motion $\tilde{\tau}$ and value of the Hamiltonian $\tilde{H}$. For a given value of g, the related value $\hat{g}$ can be determined through numerical solution of $\tilde{H}(\tilde{\tau}; g) = \tilde{H}(\tilde{\tau}; \hat{g})$, i.e.

$$\frac{\ln F(\tilde{\tau}; g)}{-2g(g+1)} = \frac{\ln F(\tilde{\tau}; \hat{g})}{-2\hat{g}(\hat{g}+1)}, \tag{3.24}$$

for a specified value of $\tilde{\tau}$. In Fig. 6a we show the relationship between g and $\hat{g}$ for representative values of $\tilde{\tau}$. The corresponding self-similar triangle motion for a particular example are shown in Fig. 11c,d. In Fig. 6b we show an alternate view of the multivaluedness of (3.19) as a function of g by plotting $\tilde{\tau}$ as a function of g for fixed values of $\tilde{H}$.

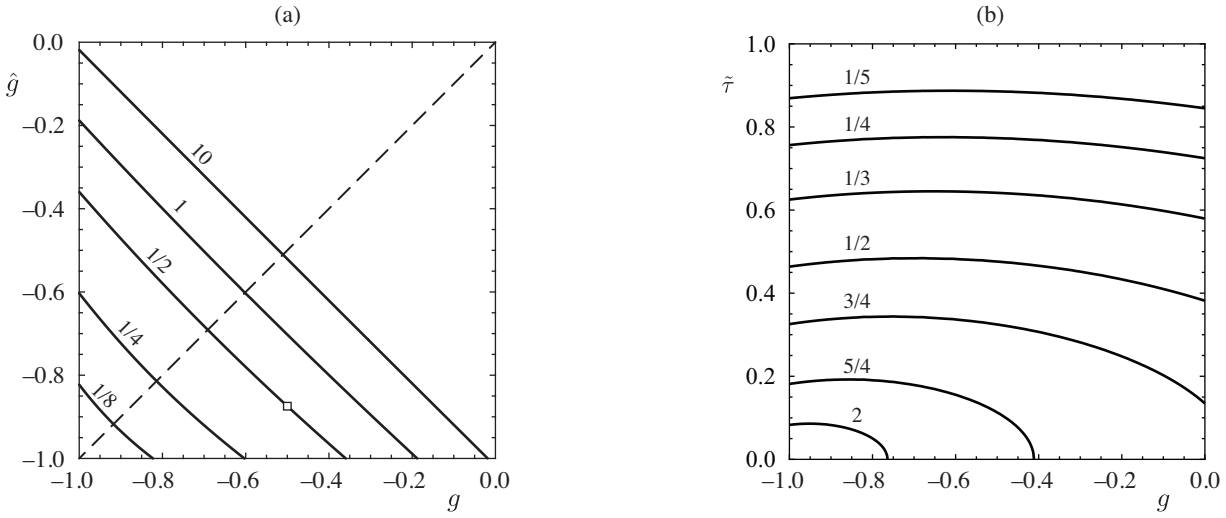

Fig. 6. (a) Values of g and $\hat{g}$ giving two different configurations with the same values of $\tilde{\tau}$ and $\tilde{H}$, determined numerically. Curves are labeled according to the corresponding value of $\tilde{\tau}$; note that the value of $\tilde{H}$ is not constant along these lines. The dashed line is the trivial case $g = \hat{g}$. The square symbol marks a representative case with $g = -1/2$, $\hat{g} \approx -0.874$, $\tilde{\tau} = 1/2$, and $\tilde{H} = \ln(8/5)$; trajectories for this case are shown in Fig. 11(c,d). (b) Values of $\tilde{\tau}$ as a function of g for various values of $\tilde{H} =$ constant; curves are labeled according to the corresponding value of $\tilde{H}$.

3.5. Self-similar motion of the vortex triangles

The description of the motion of the vortex triangle can be completed by specifying the motion of its circumcenter Z and its orientation as given by φ_1, which can be determined through (2.14e) and (2.14f) respectively. These equations take on a simplified form during self-similar motion since the angles A, B, C are constant. Let us define the dimensionless quantities

$$\tilde{t} = \frac{t}{\tau} \quad \text{and} \quad \tilde{Z} = \frac{Z}{R_0}, \tag{3.25}$$

so that collapsing solutions with $\tau > 0$ have $\tilde{t} > 0$ and expanding solutions with $\tau < 0$ have $\tilde{t} < 0$. By this non-dimensionalization, the time of collapse corresponds to $\tilde{t} = 1$. We can then re-write (2.14f) and (2.14e), respectively as

$$\frac{\mathrm{d}\varphi_1}{\mathrm{d}\tilde{t}} = \frac{\tilde{\tau} K_1}{1 - \tilde{t}}, \tag{3.26a}$$

$$\frac{\mathrm{d}\tilde{Z}}{\mathrm{d}\tilde{t}} = \tilde{\tau} K_2 \, \frac{\mathrm{e}^{\mathrm{i}\varphi_1(\tilde{t})}}{\sqrt{1 - \tilde{t}}}, \tag{3.26b}$$

where K_1 and K_2 are constants given by

$$K_1 = -\frac{\sin^2(A-B) + \sin^2(B-C) + \sin^2(C-A)}{4\sin(A-B)\,\sin B\,\sin C\,\sin(C-A)}, \tag{3.27a}$$

$$K_2 = \frac{\sin 2(A-B) + \sin 2(B-C) + \sin 2(C-A) + 8\cos B\,\sin^3 B - 8\cos C\,\sin^3 C}{8\sin(A-B)\,\sin B\,\sin C\,\sin(C-A)}$$
$$+ \mathrm{i}\,\frac{-2\sin^2 A + \sin^2 2B + \sin^2 2C + \sin^2(A-B) - \sin^2(B-C) + \sin^2(C-A)}{4\sin(A-B)\,\sin B\,\sin C\,\sin(C-A)}. \tag{3.27b}$$

Integrating (3.26a), we obtain $\varphi_1(\tilde{t})$ and $\tilde{Z}$ as

$$\varphi_1(\tilde{t}) = -\tilde{\tau} K_1 \log\left(1 - \tilde{t}\right) \tag{3.28a}$$

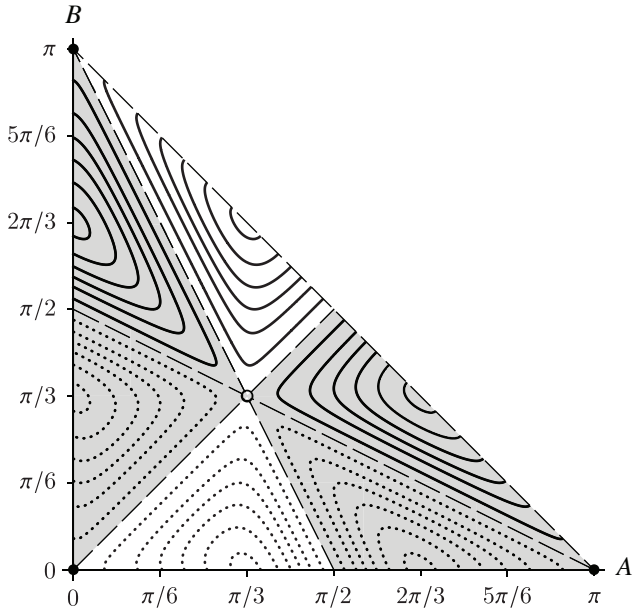

Fig. 7. Level curves of $\tilde{s}(1)$ (solid lines) and $\tilde{s}(-1)$ (dotted lines) in the (A, B) plane, with $C = \pi - A - B$. Symbols, limiting lines and shading follow the conventions in Figs. 3 and 4a.

$$\tilde{Z}(\tilde{t}) = -\tilde{\tau} K_2 \frac{\left(1-\tilde{t}\right)^{1/2-\mathrm{i}\tilde{\tau}K_1}}{1/2-\mathrm{i}\tilde{\tau}K_1}. \tag{3.28b}$$

Here we have set $\varphi_1(0) = 0$, so that the line joining z_1 and Z is initially horizontal, and $\tilde{Z}(1) = 0$, so that the vortices collapse into the origin of co-ordinates. This latter choice is equivalent to taking the center of vorticity (2.11) to coincide with the origin of co-ordinates, i.e. with taking $z_{cv} = 0$. As noted in [16], the circumcircle always passes through the point z_{cv}, and thus the point of collapse must lie on the boundary of the original circumcircle.

The distance traveled by the circumcenter is the arc length of the path of $\tilde{Z}(\tilde{t})$,

$$\tilde{s}(\tilde{T}) = \int_0^{\tilde{T}} \left| \frac{\mathrm{d}\tilde{Z}}{\mathrm{d}\tilde{t}} \right| \mathrm{d}\tilde{t}, \tag{3.29a}$$

which gives a representation of the distance traveled by the vortex triangle during the time interval $0 \le \tilde{t} \le |\tilde{T}|$. The sign in (3.29a) is chosen according to whether the configuration is collapsing (positive) or expanding (negative). By substituting (3.26b) into (3.29a) and performing the integration we see that

$$\tilde{s}(\tilde{T}) = 2\tilde{\tau}\ |K_2| \left(1 - \sqrt{1-\tilde{T}}\right), \tag{3.29b}$$

with $\tilde{\tau} > 0$, $0 < \tilde{T} \le 1$ for self-similar collapse and $\tilde{\tau}, \tilde{T} < 0$ for self-similar expansion. In particular we see that

$$\tilde{s}(1) = 2\tilde{\tau}\ |K_2| \tag{3.29c}$$

is the distance traveled by the circumcenter during the time it takes for a configuration to collapse, and

$$\tilde{s}(-1) = 2\tilde{\tau}\ |K_2| \left(1 - \sqrt{2}\right) > 0 \tag{3.29d}$$

is the distance traveled during expansion over the same unit of time. Representative level curves of $\tilde{s}(1)$ and $\tilde{s}(-1)$ in the (A, B) plane are shown in Fig. 7. Since the point of collapse always occurs on the boundary of the initial (dimensionless) circumcircle with radius one, it must be true that $\tilde{s}(1) \ge 1$; numerically we find that $\tilde{s}(1) > 2$.

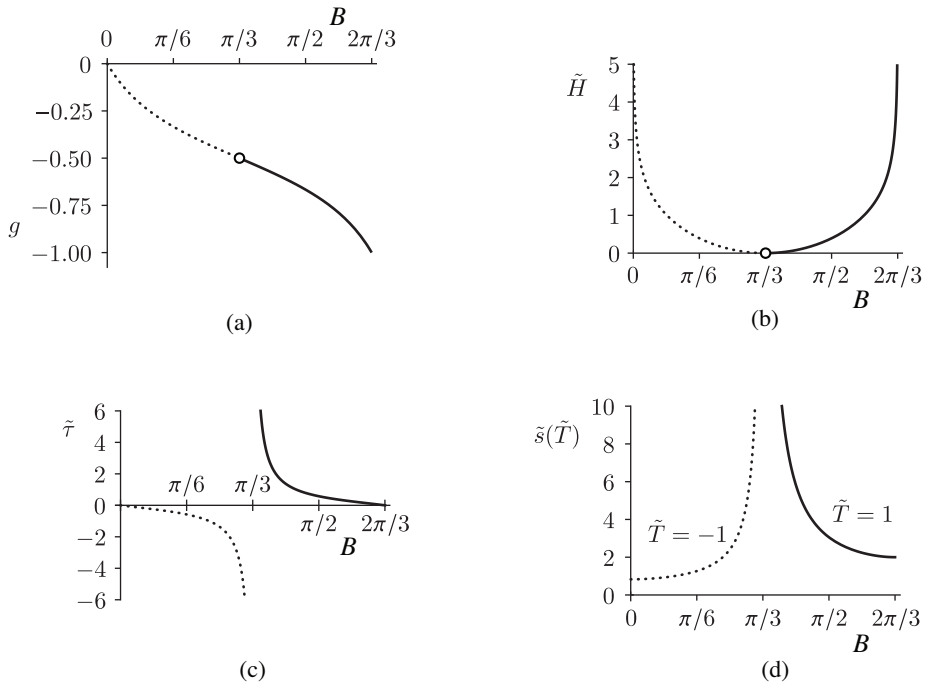

Fig. 8. Values of (a) g, (b) $\tilde{H}$, (c) $\tilde{\tau}$ and (d) $\tilde{s}(\tilde{T})$, with $\tilde{T} = \pm 1$, as functions of B for the special case $A = \pi/3$. The solid lines denote collapsing solutions and the dotted lines denote expanding solutions. The open circles mark the equilibrium configurations for which $B = \pi/3$.

3.6. Examples of self-similar motion

One may plot examples of self-similar motion by fixing as constant either g, $\tilde{H}$ or $\tilde{\tau}$ and following along a curve in Fig. 3 or Fig. 4a. Here we choose instead to explore the solution space 'centered' on the equilibrium configuration $(A, B) = (\pi/3, \pi/3)$ by fixing $A = \pi/3$. Equations (3.12), (3.13c) and (3.15) then become expressions for g, $\tilde{H}$ and $\tilde{\tau}$, respectively, as functions of B alone. These quantities vary continuously as functions of B for $0 < B < 2\pi/3$, except for an isolated singularity at $B = \pi/3$, as shown in Fig. 8. The singularity in $g(B)$ at $B = \pi/3$ occurs since there exists an equilibrium configuration for every value of g. The Hamiltonian $\tilde{H} = 0$ for the equilibrium configurations, and $\tilde{H} \to \infty$ for the singular configurations corresponding to $B = 0$ or $B = 2\pi/3$ (for $A = \pi/3$). It is clear from Fig. 8b that $\tilde{H}$ attains its minimum of zero when the vortices are in equilibrium (at $B = \pi/3$), and is positive for self-similar motion. This result is consistent with [23]. It is to be expected that $\tilde{\tau} \to \infty$ for the equilibrium configurations; we also see that $\tilde{\tau} \to 0$ for the singular configurations with $B = 0, 2\pi/3$, which we discuss more below.

Figure 9 shows a selection of collapsing configurations for $A = \pi/3$ and $-1 < g < -1/2$. For g near $-1/2$, the vortex configuration is near that of an equilateral triangle, and the configuration rotates about the center of vorticity many times before collapsing. As $g \to -1$, we have $C \to 0$ and $B \to 2\pi/3$, the distance between vortices 1 and 2 approaches zero, the strengths of vortices 1 and 2 approach being equal and opposite, and the strength of vortex 3 becomes large relative to the other two vortices. The configuration in this limit can be approximated as a small vortex dipole (vortices 1 and 2) moving in the field of a strong, fixed vortex (vortex 3). Although the strengths of the dipole vortices are small relative to vortex 3, their separation is approaching zero, giving rise to a large self-induced propagation speed of the dipole toward vortex 3; for $A = \pi/3$, this self-induced motion is at an angle of $\pi/3$ relative to the motion induced by vortex 3. Since we take $\Gamma_1 > 0$, in the limit as $g \to -1$ the dipole self-propagation speed becomes infinite, leading to $\tilde{\tau} \to 0$.

Representative expanding configurations for $A = \pi/3$ and $-1/2 < g < 0$ are shown in Fig. 10. These expanding configurations are related to the collapsing configurations in Fig. 9 by the transformation (3.11). As illustrated in Fig. 8, the dimensionless quantities $\tilde{H}$ and $|\tilde{\tau}|$ remain

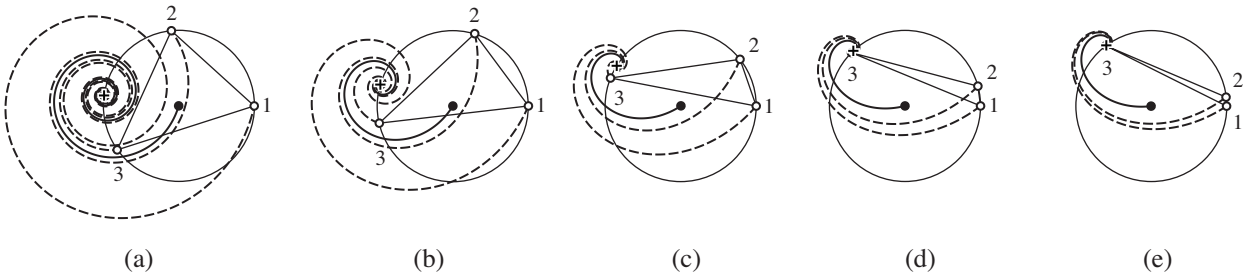

Fig. 9. Examples of self-similar collapse of three vortices with $A = \pi/3$ and $g =$ (a) $-9/16$, (b) $-5/8$, (c) $-3/4$, (d) $-7/8$, and (e) $-15/16$. Triangles and circumcircles are shown with light solid lines. Open circles mark the initial vortex positions, labeled by vortex number; closed circles mark the initial position of the circumcenter; and the + symbols mark the point of collapse. Vortex trajectories are shown with dashed lines, and circumcenter trajectories are shown with heavy solid lines. For each triangle, the circumcircle has initial radius $R_0 = 1$, $\Gamma_1 = 1$, and $A = \pi/3$; the remaining parameters for each example are (a) $(\Gamma_2, \Gamma_3) = (-16/9, -16/7)$, $(B, C) \approx (72.2^\circ, 47.8^\circ)$, $\tilde{H} \approx 0.061$, $\tilde{\tau} \approx 1.705$; (b) $(\Gamma_2, \Gamma_3) = (-8/5, -8/3)$, $(B, C) \approx (83.4^\circ, 36.6^\circ)$, $\tilde{H} \approx 0.232$, $\tilde{\tau} \approx 0.819$; (c) $(\Gamma_2, \Gamma_3) = (-4/3, -4)$, $(B, C) \approx (100.9^\circ, 19.1^\circ)$, $\tilde{H} \approx 0.795$, $\tilde{\tau} \approx 0.325$; (d) $(\Gamma_2, \Gamma_3) = (-8/7, -8)$, $(B, C) \approx (112.4^\circ, 7.6^\circ)$, $\tilde{H} \approx 1.627$, $\tilde{\tau} \approx 0.126$; and (e) $(\Gamma_2, \Gamma_3) = (-15/16, -16)$, $(B, C) \approx (116.6^\circ, 3.4^\circ)$, $\tilde{H} \approx 2.340$, $\tilde{\tau} \approx 0.058$.

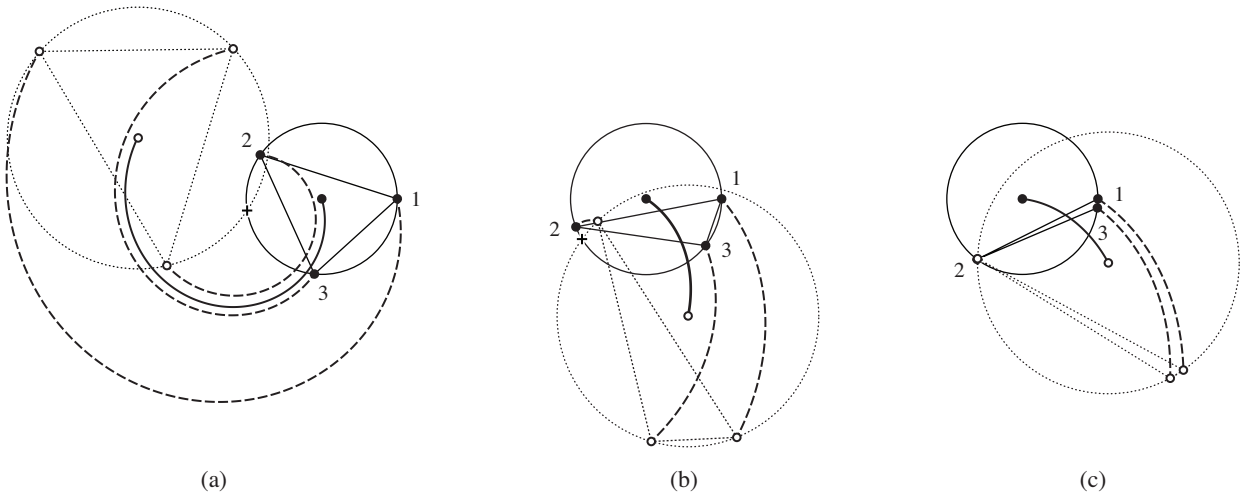

Fig. 10. Examples of self-similar expansion for $0 \geq \tilde{t} \geq -2$ with $A = \pi/3$ and $g =$ (a) $-9/16$, (b) $-1/4$, (c) $-1/16$. Corresponding collapsing configurations are shown in Fig. 9, with detailed parameters given in the caption: panel (a) corresponds to Fig. 9a, panel (b) to Fig. 9c, and panel (c) to Fig. 9e. Initial triangles and circumcircles are shown with light solid lines, and final triangles and circumcircles at $\tilde{t} = -2$ are shown with dotted lines. Vortex trajectories are shown with dashed lines, and circumcenter trajectories are shown with heavy solid lines. Closed circles mark the initial positions of the circumcenters and the vortices, which are labeled by vortex number; open circles mark the final positions of the circumcenters and the vortices. The + symbols mark the center of vorticity; in panel (c) the z_{cv} nearly corresponds with vortex 2, and the + symbol is obscured by the circle marking the vortex position.

unchanged in this transformation, but the expanding configurations travel less distance per unit time than the corresponding collapsing configurations. Of course, the collapsing configurations travel only a finite distance before collapse, while the expanding configurations do so with $\tilde{s} \to \infty$.

As discussed in §3.4, for given values of $\tilde{\tau}$ and $\tilde{H}$ there exist two values of g that satisfy (3.19), and thus there are two different configurations with the same time of collapse and same energy. Two particular cases of this situation are shown in Fig. 11. The trajectories in Fig. 11a,b correspond to the case marked by an open square in Fig. 4c. The trajectories in Fig. 11c,d correspond to the case marked in Fig. 6a.

Fig. 11. Two representative cases of self-similar collapse in which two different configurations have the same values of $\tilde{\tau}$ and $\tilde{H}$. In panels (a,b), $\tilde{\tau} \approx 0.250$ and $\tilde{H} \approx 1.009$ with (a) $g = -3/4$ and (b) $g = -7/8$; in panels (c,d), $\tilde{\tau} = 1/2$ and $\tilde{H} = \ln(8/5) \approx 0.470$ with (c) $g = -1/2$ and (d) $g \approx -0.874$.

4. SUMMARY, DISCUSSION AND OUTLOOK

A detailed study of self-similar motion of three point vortices in the plane has been made using the recently developed geometrical formulation [16] that represents the vortex configuration in terms of the interior angles of the triangle formed by the vortices, $\{A, B, C\}$; the center and radius of the circle that circumscribes that triangle, $\{Z, R\}$; and the orientation of the triangle, as given by φ_1. With the constraint on the interior angles, namely $A + B + C = \pi$, this representation yields a six-dimensional system of ODEs that can be solved, in general, to completely determine the vortex motion. The only exception is when the vortices become colinear, in which case this geometrical representation becomes singular and the original vortex equations of motion must be used to continue the solution. When only the vortex triangle size and shape are of interest, one can consider instead the embedded four-dimensional subsystem consisting of $\{R, A, B, C\}$.

The new geometrical approach and the ensuing results complement the many previous studies [1, 12, 22, 31] that focused on representing the configuration in terms of the lengths of the triangle sides, $\{s_1, s_2, s_3\}$, and the area of the triangle, Δ. In this classic approach [1, 12, 22, 31], if the vortices become colinear the addition of an equation for $\mathrm{d}\Delta/\mathrm{d}t$ closes the system of equations, enabling continuation of the solutions through the colinear singularity. As noted above, a similar closure is not possible in the present geometrical approach. In contrast, determining the location and orientation of the vortex triangle in the classic approach requires use of the original vortex equations of motion, while in the present approach these variables are included in the closed formulation.

Studying the self-similar motion of three point vortices using this new geometrical approach [16] has produced several results that were not found previously using the classic formulation. The symmetries inherent in the system have been exploited to reduce the parameter space of vortex strengths significantly; all possible self-similar motions can be explored by considering only $-1 < g < 0$. An implicit expression relating the time of collapse and the Hamiltonian energy of the system has been derived and studied, and the results appear consistent with the one available numerical example from [17]. It is found that the time of collapse is a single-valued function of the Hamiltonian energy, and the parameter g is a double-valued function of the time of collapse and the Hamiltonian energy. The latter statement means that for every choice of the time of collapse (or characteristic time) and the energy, there exists two different collapsing (or expanding) configurations with two different values of g. The time of collapse $\tilde{\tau}$ is largest (approaching infinity) for initial configurations that are close to the equilateral triangle or colinear relative equilibrium configurations, and smallest (approaching zero) for initial configurations that are close to configurations consisting of a vortex dipole in the field of a strong vortex. Explicit expressions are derived for the total distance travelled by the circumcenter in self-similar motion. Several examples analyzing these various aspects of the self-similar motion have been presented.

The self-similar solutions for three point vortices have found application in related areas of fluid mechanics such as turbulence theory in two-dimensions. A recent series of papers [10, 11, 29] discuss a possible explanation for the anomalous enstrophy dissipation in two-dimensional turbulent flow through self-similar collapse of α- and ε-point vortices. These extensions of the point vortex model regularize the velocity field, with α and ε as the regularization parameters, and they become the point vortex model in the limit as $\alpha \to 0$ or $\varepsilon \to 0$; ε-point vortices are a generalization of the α-point vortices. In this limit, the authors find that a system of three ε-point vortices undergoes

self-similar collapse and dissipates the enstrophy [10, 11, 29]. The condition for this collapse is shown explicitly to be only $\gamma_2 = 0$ [11]. However, in their general formulation they assume that $L = \mathcal{O}(\varepsilon)$, so that they also have $L \to 0$ in the $\varepsilon \to 0$ limit. We may interpret their model(s) as the smearing out of initial conditions that lead to collapse, due to the regularized velocity field of the ε-point vortices. They are able to continue past the finite-time singularity of collapse into expanding configurations using the limit of the regularized solution [10], which is not possible in the point vortex formulation.

The finite-time collapse and burst (i.e. self-similar expansion) motions of three vortices is a particular case of finite-time N-vortex collapse. For $N = 3$, the necessary and sufficient conditions for such motion show that they are always self-similar. This fact has been recognised in the literature [1, 23], and the present work provides a complementary proof for it. Self-similar motion of $N = 4$ and $N = 5$ vortices has been explored; however, it is unclear whether self-similar motion is the only possible form of collapse and burst motions for these larger systems [23, 25]. For larger values of N, the collapse and burst motions of special configurations in the plane such as vortex triple rings [15, 26] and vortex lattices [24] have been explored. Some numerical observations have been made relating vortex lattice collapse to three-vortex collapse [24], and there have also been some numerical studies on the self-similar collapse of $N > 3$ vortices [17]. However, many questions remain unanswered: is self-similar collapse the only possible type of collapse for $N > 3$ vortices in the plane? How robust are the initial conditions leading to collapse [20]? Further studies are required to answer these questions; in particular, it is not clear what similar geometrical methods can be used to treat N vortex collapse for $N > 3$.

ACKNOWLEDGMENTS

V.S.K. acknowledges financial support from CAPES/Brazil through a Science Without Borders postdoctoral program during his stay at the Federal University of Pernambuco, and the ESI Junior Research Fellowship Program during his stay at the Erwin Schrodinger International Institute for Mathematics and Physics, University of Vienna.

REFERENCES

1. Aref, H., Motion of three vortices, *Physics of Fluids*, 1979, vol. 22, pp. 393–400.
2. Aref, H., Integrable, chaotic and turbulent vortex motion in two-dimensional flows, *Annual Review of Fluid Mechanics*, vol. 15, pp. 345–389, 1983.
3. Aref, H., Three-vortex motion with zero total circulation: Addendum, *Journal of Applied Mathematics and Physics (ZAMP)*, 1989, vol. 40, pp. 495–500.
4. Aref, H., A transformation of the point vortex equations, *Physics of Fluids*, 2002, vol. 14, pp. 2395–2401.
5. Aref, H., Self-similar motion of three point vortices, *Physics of Fluids*, 2010, vol. 22, no. 057104, 12 pp.
6. Aref, H., Rott, N., and Thomann, H., Gröbli's solution of the three-vortex problem, *Annual Review of Fluid Mechanics*, 1992, vol. 24, pp. 1–20.
7. Batchelor, G. K., *An Introduction to Fluid Dynamics*, Cambridge: Cambridge University Press, 1967.
8. Borisov, A. V. and Palmov, A. E., Dynamics and statics of vortices on a plane and a sphere – I, *Regular and Chaotic Dynamics*, 1998, vol. 3, no. 1, pp. 28–38.
9. Coxeter, H. S. M., *Introduction to Geometry*, 2nd. ed., Wiley, 1969.
10. Gotoda, T. and Sakajo, T., Distributional enstrophy dissipation via the collapse of three point vortices, *Journal of Nonlinear Science*, 2016, vol. 26, 1525–1570.
11. Gotoda, T. and Sakajo, T., Universality of the anomalous enstrophy dissipation at the collapse of three point vortices on Euler-Poincaré models, *SIAM J. Appl. Math.*, 2018, vol. 78, no. 4, pp. 2105–2128.
12. Gröbli, W, *Spezielle probleme über die Bewegung geradliniger paralleler Wirbelfäden*, Zürich: Zürcher und Furrer, 86 pp.; see also: *Vierteljahrsschrift der Naturforschenden Gesellschaft in Zürich*, 1877, vol. 22, pp. 37-81, 129-165.
13. Helmholtz, H. von, Über Integrale der hydrodynamischen Gleichungen, welche den Wirbelbewegungen entsprechen, *J. Reine Angew. Math.*, 1858, vol. 55, pp. 25–55; see also: Tait, P.G., On integrals of the hydrodynamical equations, which express vortex-motion, *Philos. Mag.*, 1867, vol. 4, no. 33, pp. 485–512.
14. Kimura, Y., Similarity solution of two-dimensional point vortices, *J. Phys. Soc. Japan*, 1987, vol. 56, no. 6, pp. 2024–2030.
15. Koiller, J., Pinto De Carvalho, S., Rodrigues Da Silva, R. and Gonçalves De Oliveira, L. C., On Aref's vortex motions with a symmetry center, *Physica D: Nonlinear Phenomena*, 1985, vol. 16, pp. 27–61.
16. Krishnamurthy, V. S., Aref, H. and Stremler, M. A., Evolving geometry of a vortex triangle, *Physical Review Fluids*, 2018, vol. 3, no. 024702, 17 pp.

17. Kudela, H., Self-similar collapse of n point vortices, *Journal of Nonlinear Science*, 2014, vol. 24, pp. 913–933.
18. Lamb, H., *Hydrodynamics*, 6th ed., Cambridge: Cambridge University Press, 1932.
19. Leoncini, X., Kuznetsov, L., and Zaslavsky, G. M., Motion of three vortices near collapse, *Physics of Fluids*, 2000, vol. 12, no. 8, pp. 1911–1927.
20. Lewkovicz, M., On the existence of finite collapsing systems of plane vortices, *Journal of Theoretical and Applied Mechanics*, 2014, vol. 52, pp. 1047–1059.
21. Newton, P. K., *The N-vortex Problem: Analytical Techniques*, *Applied Mathematical Sciences*, vol. 145, New York: Springer-Verlag, 2001.
22. Novikov, E. A., Dynamics and statistics of a system of vortices, *Soviet Physics JETP*, 1975, vol. 41, pp. 937–943.
23. Novikov, E. A. and Sedov, Yu. B., Vortex collapse, *Soviet Physics JETP*, 1979, vol. 50, no. 2, pp. 297–301.
24. O'Neil, K. A., Collapse of point vortex lattices, *Physica D: Nonlinear Phenomena*, 1989, vol. 37, pp. 531–538.
25. O'Neil, K. A., Relative equilibrium and collapse configurations of four point vortices, *Regular and Chaotic Dynamics*, 2007, vol. 12, pp. 117–126.
26. O'Neil, K. A., Relative equilibrium and collapse configurations of heterogeneous vortex triple rings, *Physica D: Nonlinear Phenomena*, 2007, vol. 236, pp. 123–130.
27. Rott, N., Three-vortex motion with zero total circulation, *Journal of Applied Mathematics and Physics (ZAMP)*, 1989, vol. 40, pp. 473–494 (With an Addendum by H. Aref [3]).
28. Saffman, P. G., *Vortex Dynamics*, Cambridge: Cambridge University Press, 1992.
29. Sakajo, T., Instantaneous energy and enstrophy variations in Euler-alpha point vortices via triple collapse, *Journal of Fluid Mechanics*, 2012, vol. 702, 188–214.
30. Schaeffer, A. C., Existence theorem for the flow of an ideal incompressible fluid in two dimensions, *Transactions of the American Mathematical Society*, 1937, vol. 42, pp. 497–513.
31. Synge, J. L., On the motion of three vortices, *Canadian Journal of Mathematics*, 1949, vol. 1, pp. 257–270.
32. Tavantzis, J. and Ting, L., The dynamics of three vortices revisited, *Physics of Fluids*, 1988, vol. 31, no. 6, pp. 1392–1409.
33. Vosbeek, P. W. C., van Geffen, J. H. G. M. ,Meleshko, V. V., and van Heijst, G. J. F., Collapse interactions of finite-sized two-dimensional vortices, *Physics of Fluids*, 1997, vol. 9, no. 11, pp. 3315–3322.